The Journal of Experimental Biology 211, 423-432
Published by The Company of Biologists 2008
doi:10.1242/jeb.011791

# Active control of free flight manoeuvres in a hawkmoth, *Agrius convolvuli*

Hao Wang[1,2,*], Noriyasu Ando[1] and Ryohei Kanzaki[1]

[1]Research Center for Advanced Science and Technology, the University of Tokyo, Tokyo, Japan and [2]Japan Society for the Promotion of Science (JSPS), Tokyo, Japan

*Author for correspondence (e-mail: wang@brain.imi.i.u-tokyo.ac.jp)

Accepted 10 November 2007

## SUMMARY

**By combining optical triangulation with the comb-fringe technique and dual-channel telemetry, wing kinematics and body attitudes accompanying muscle activities of free-flying male hawkmoths were recorded synchronously when they performed flight manoeuvres elicited by a female sex pheromone. The results indicate that the wing leading edge angular position at the ventral stroke reversal, which can be decomposed by two orthogonal angular parameters (a flapping angle and a deviation angle), is well controllable. Two specific flight muscles, the dorsal-ventral muscle (DVM, indirect muscle, a wing elevator) and the third axillary muscle (3AXM, direct muscle, a wing retractor), can modulate the flapping angle and the deviation angle, respectively, by means of regulating the firing timing of muscle activities. The firing timing can be expressed by the firing latency absolutely, which is just before the timing of ventral stroke reversal. The results illustrate that lengthening the firing latency of the DVM and of the 3AXM can increase the flapping angle and the deviation angle, respectively, which both strengthen the downstroke at the ventral stroke reversal. The relationship of bilateral asymmetry shows that the bilateral differences in the firing latency of the DVM and of the 3AXM will cause bilateral differences in the wing position, which accompany the variations of yaw and roll angles in time course. This implies the contribution of the two muscles to active steering controls during turning or banking, though the DVM being an indirect muscle was generally treated as a power generator. Finally, the relationship between the pitch angle and the 3AXM latency, deduced from the relationships between the pitch angle and the deviation angle and between the deviation angle and the 3AXM latency, shows that lengthening the 3AXM latency can increase the pitch angle at the ventral stroke reversal by moving the wing tip far away from the centre of gravity of the body, which indicates a functional role of the 3AXM in active pitching control.**

Key words: free flight, flight control, electromyography, wing kinematics, hawkmoth.

## INTRODUCTION

Understanding how flight muscles affect wing kinematics is an interim stage to discovering the mechanisms of active flight control. Several species of insect (Hedwig and Becher, 1998; Tu and Dickinson, 1996; Wilson and Weis-Fogh, 1962; Wolf, 1990) have been studied in tethered conditions, including the hawkmoth *Manduca sexta* (Kammer, 1971). Based on anatomical studies of hawkmoths (Eaton, 1971; Rheuben and Kammer, 1987), three kinds of flight muscle have been well studied in tethered hawkmoths: the dorsal longitudinal muscle [DLM, $DL_1$; a wing depressor; nomenclature after Eaton (Eaton, 1971)], the dorsal-ventral muscle [DVM, $DV_1$; a wing elevator; nomenclature after Eaton (Eaton, 1971)] and the third axillary muscle [3AXM, upper bundle; a wing retractor; nomenclature after Rheuben and Kammer (Rheuben and Kammer, 1987)]. The DLM and the DVM are indirect muscles, which deform the exoskeleton of the thorax and actuate the wing indirectly. The activity of the DLM is generally treated as the time reference for each wingbeat, considering its relative regularity and bilateral symmetry. The 3AXM, which is a direct muscle and retracts the wing directly, is known as a 'steering muscle' because its activity is changeable during turning manoeuvres in tethered flight (Kammer, 1971; Rheuben and Kammer, 1987).

In natural free flight, hawkmoths can express many flight behaviours including hovering in front of and feeding from flowers, forward and backward flight, obstacle avoidance, decelerating upon approach and compensating for any slight perturbations to their positions or orientations (Stevenson et al., 1995). Until now, the wireless transmission of muscle potentials has been applied for freely flying desert locusts (Fischer and Kutsch, 1999; Kutsch, 2002; Kutsch et al., 2003) and hawkmoths (Ando and Kanzaki, 2004). The flight muscle activities and wing kinematics [such as wingbeat frequency, the firing relationship of elevation muscles and the correlation between muscle activities and body/wing kinematics (Kutsch, 2002; Kutsch et al., 2003)] during free flight of locusts could be different from those in tethered flight. As for hawkmoths during free flight, the flight muscle activities are much less changeable than those during tethered flight, suggesting that slight modulation of the motor output pattern and the subsequent wing kinematics might be adequate for free flight manoeuvres. The telemetric recording of muscle potentials during free flight revealed that the activities of the DVM and the 3AXM are less variable than those in tethered flight; however, they are activated in phase with wingstroke regularly just before the ventral stroke reversal (Ando and Kanzaki, 2004). These observations suggest that hawkmoths may control the wing position at the ventral stroke reversal through the two muscles, given that they are both synchronous (neurogenic) flight muscles (Rheuben and Kammer, 1987). Considering the closed-loop control system of free flight *versus* the open-loop control system of tethered flight, it is necessary to analyse both flight muscle physiology and wing kinematics simultaneously during free flight.

In this study, three kinds of flight muscle, the DLM, DVM and 3AXM, were selected based on previous anatomical and tethered

flight studies of hawkmoths (Eaton, 1971; Rheuben and Kammer, 1987). We recorded EMGs during free flight manoeuvres of male hawkmoths towards a female-extracted sex pheromone source, and the corresponding wing positions at the ventral stroke reversal were quantified in a body-fixed coordinate frame using the projected comb-fringe technique (Wang et al., 2003). We investigated the potential relationships between the quantified variables and the muscle activities and found that the DVM and 3AXM contributed to different parameters of wing kinematics, and the bilateral symmetry and asymmetry of muscle activities further elucidated the functions of these muscles in active control during free flight manoeuvres.

## MATERIALS AND METHODS

This study was carried out during May and June 2006 at the University of Tokyo, Tokyo, Japan. To capture free flight manoeuvres of the hawkmoth and to record the corresponding EMG signals from flight muscles simultaneously, we integrated experimental systems combining optics and telemetry subsystems (Fig. 1), similar to previous studies (Ando et al., 2002; Wang et al., 2003).

### Animals

Two to four day old adult sweet potato hawkmoths, *Agrius convolvuli* (Lepidoptera: Sphingidae; L.), were obtained from our laboratory colony, reared with artificial diets. Larvae, pupae and adult moths were kept under a 16 h:8 h light:dark cycle at 25°C. Moths were separated by sex as pupae and were housed in different incubators (MIR-253, Sanyo, Japan) under the same ambient regime and emerged within 23 cm × 23 cm × 23 cm cages. Adult female moths were used to extract a sex pheromone. The extraction was prepared by washing the tip of a virgin female moth's abdomen, which contains the sex-pheromone gland, in 60 μl of n-hexane (Wako pure chemical industries, Osaka, Japan) for 10 min, yielding '1 female equivalent' of crude pheromone extract (Kanzaki et al., 1989). Adult male moths with unmarred wings were selected to have a telemeter attached for the free flight experiments.

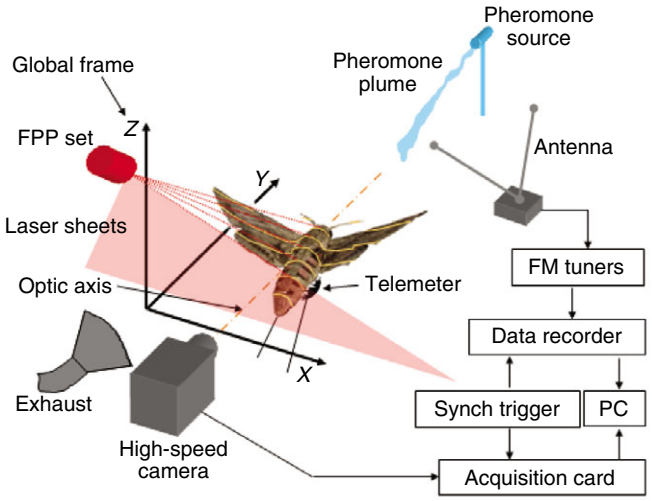


Fig. 1. Experimental setup used to record flight manoeuvres and EMG activity synchronously. Hawkmoths with a ventrally attached telemeter were released into an enclosed electromagnetically shielded flight arena and imaged with one high-speed camera associated with a fringe pattern projector (FPP) set at 1000 frames $s^{-1}$.

### Wing kinematics

The optical measurement system we used was an updated version of a previous one (Wang et al., 2003). Male hawkmoths were released into an enclosed electromagnetically shielded flight chamber 50 cm×50 cm×60 cm in size. One high-speed camera (Fastcam-512PCI, Photron, Japan; 1000 frames $s^{-1}$, shutter speed 0.25 ms, resolution 512 pixels × 512 pixels) was aimed at a small region in front of a pheromone-baited target. Correspondingly, one near-infrared laser fringe pattern projector (FPP; SNF-533L-785S-75-10, Stocker Yale, NH, USA; interbeam fringe angle 0.38°, λ=781.5 nm) was also aimed at this region. The angle between the optical axis of the camera and the central line of the FPP was about 45°. The back lighting required for image capture was generated by an incandescent lamp covered with an infrared-transmissible acrylic filter (λ>800 nm). The spectral ranges of the FPP and the backlight were well below the insects' sensitivity (Burkhardt, 1977) and hence did not compromise the visually mediated components of the animals' flight behaviour. From the 2-dimensional image of the hawkmoth and the deformed fringes on it (Fig. 2A), a 3-dimensional reconstruction (Fig. 2B) could be made based on optical triangulation. Given the limited deformation of the backside of the thorax, the fringe information on it could be used to improve the accuracy of the body-fixed coordinate frame. A custom-built interactive graphic user interface (developed using Matlab, The MathWorks, Inc., Natick, MA, USA) was used to extract the fringe information and then calculate the wing kinematics and locomotion in local and global frames.

There are many parameters to describe wing kinematics and locomotion in insect flight, such as stroke amplitude and angle of attack (Willmott and Ellington, 1997). In this study, we focused on parameters that could express the wing leading edge angular positions at the ventral stroke reversals. These positions were attractive because the DVM and 3AXM activated just ahead of this (Ando and Kanzaki, 2004) as well as because of their variability. Here we defined the wing leading edge angular positions at ventral stroke reversals by two angles, the flapping angle ($\Phi$) and the deviation angle ($\Psi$), in the body-fixed coordinate frame (Fig. 3A). Decomposing wing position by the two orthogonal angular parameters along the coordinate axes in the body-fixed frame is coincident with the anatomical structures of the DVM and 3AXM (Eaton, 1971); that is, the directions of the muscles' contraction are nearly parallel to the local coordinate axes. The corresponding bilateral differences, treating the left side as the reference, were exhibited by $\Delta\Phi$ and $\Delta\Psi$, respectively. During free flight, a hawkmoth is always oscillating its body axis, which continuously affects flight attitudes aloft. In the present study, we treated the recording frames in which the ventral stroke reversals were present as key frames. The locomotion parameters such as pitch angle and the centre of the body-fixed coordinate frame were calculated based on the key frames and treated as representatives of the current wingbeat cycle though they were changeable in reality. This treatment simplified data processing, and did not compromise the comparability among wingbeat cycles because the key frame represents the identical time in each period of wing movement.

### Telemetry

The two-channel FM telemeter employed here was revised from a previous one (Ando et al., 2002). The weight of the telemeter, which was 0.23 g including a 0.13 g battery (SR416SWEC, Toshiba battery, Saku, Nagano, Japan), occupied about 24% of the weight of the investigated male hawkmoths (0.94±0.05 g, mean ± s.d., $N$=7). Though the animals could perform manoeuvres freely,

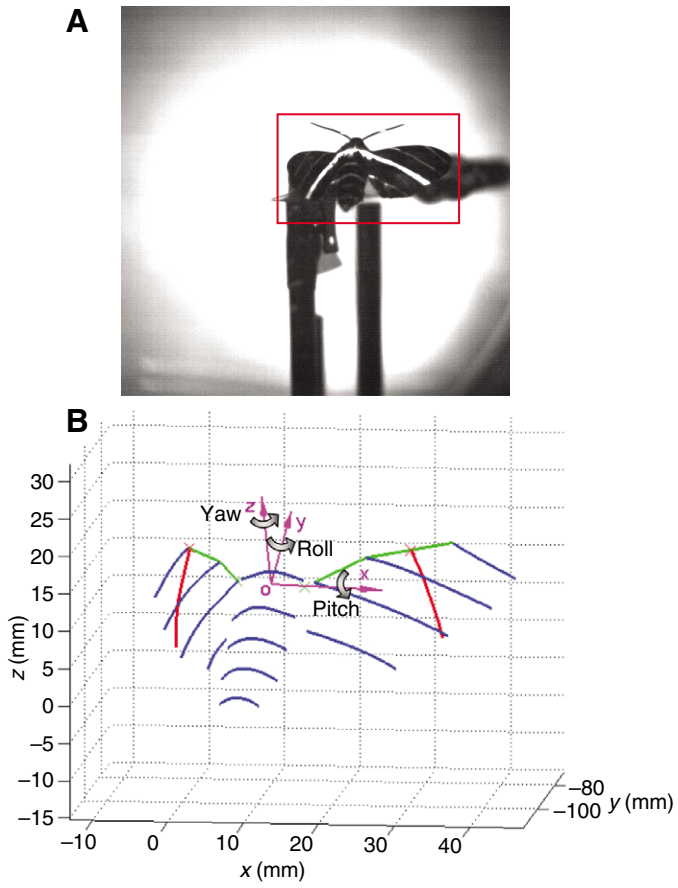


Fig. 2. Three-dimensional reconstruction of optical fringes and body-fixed coordinate frame. (A) One example of a recording frame with the deformed fringes on the wings (back view, elevation=azimuth=0°). The brightest one was the reference fringe. (B) Surface topography of body and wings by three-dimensional reconstruction (rear lateral view, elevation=10°, azimuth=7°). Blue curves indicate the reconstructed laser fringes; green curves, lateral leading edges; red curves, 50% cross-section along wingspan. Green crosses indicate wing bases; red crosses, middle points of leading edges. Body-fixed coordinate frame (magenta vectors) deduced by three-dimensional reconstruction is also superimposed. Euler angles are indicated by the grey curved arrows, whose rotations have an ordered sequence of yaw ($\alpha$), pitch ($\beta$) and roll ($\gamma$) according to the Fick coordinate system (Haslwanter, 1995; Schilstra and Hateren, 1998). Signs comply with the right-hand rule, and the reference orientation is coincident with the global coordinate frame (denoted by the coordinate grid) fixed on the flight arena.

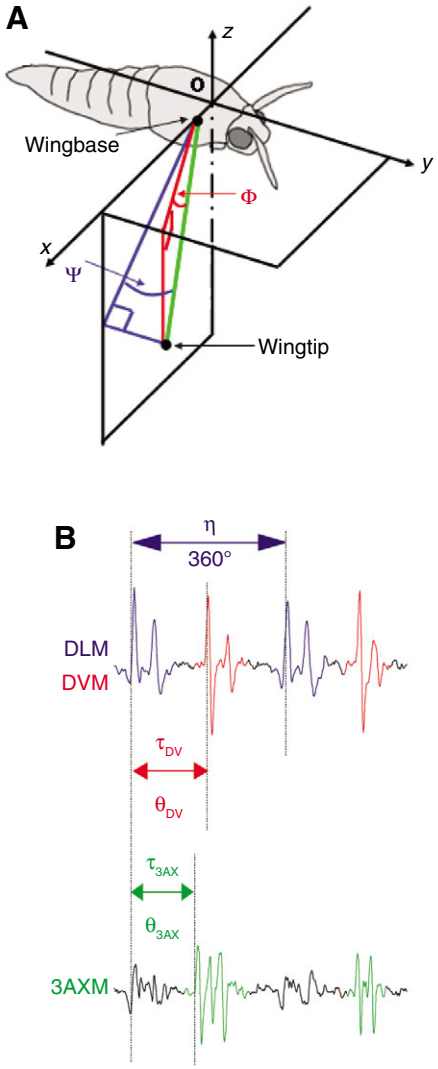


Fig. 3. Definitions of wing kinematics and muscle activities. (A) Quantification of the wing position at the ventral stroke reversal. The body-fixed coordinate frame is shown in black. The leading edge of the right forewing is indicated by a green line located in the fifth quadrant. The red and blue lines indicate the projected leading edges on the coordinate plane of *xoy* and *xoz*, respectively. Flapping angle ($\Phi$, in red) and deviation angle ($\Psi$, in blue) are defined as the included angles between the leading edge and the corresponding projection planes ($\Phi>0$ if $z<0$, $\Psi>0$ if $y>0$, and *vice versa*). The corresponding bilateral differences, treating left side as the reference, were exhibited by $\Delta\Phi$ and $\Delta\Psi$, respectively. (B) Definition of the EMG activities. Cycle length ($\eta$) is the interval between the first DLM spikes in the adjacent wingbeats, which can be understood as a half-closed–half-open interval, in which the anterior DLM reference spike was included while the posterior one was excluded. The activities of the DVM and 3AXM were expressed by the firing timing relative to the anterior DLM reference spike. DVM and 3AXM latencies ($\tau_{DV}$ and $\tau_{3AX}$) are their onset timing relative to the anterior DLM reference. DVM and 3AXM phases ($\theta_{DV}$ and $\theta_{3AX}$) are defined as the ratio of latencies to the cycle length, treating it as 360°. The corresponding bilateral differences in latency and phase, treating left side as the reference, were exhibited by $\Delta\tau$ and $\Delta\theta$, respectively.

the ventrally attached telemeter might increase the pitch angle aloft (46.22±4.23°, mean ± s.d., $N$=197 cycles, 7 insects). The effective radius of the telemeter was about 3 m, which could cover the whole experimental area. The updated telemeter circuit along with the electromagnetically shielded flight chamber improved the quality of the EMG recordings. A telemetry system and recording of EMGs were described previously (Ando and Kanzaki, 2004). Recording electrodes (copper wires of 100 μm in diameter, insulated except at the tip) were inserted into flight muscles. Simultaneous recording of both the DLM and the DVM was made by inserting a single electrode into the edge of the DLM, adjacent to the DVM (Ando and Kanzaki, 2004). Transmitted signals from the telemeter were received by two FM tuners and recorded onto a data acquisition system (Powerlab/8SP, ADInstruments, Colorado Springs, CO, USA), sampling rate 10 kHz. Only the EMG signals corresponding to satisfactory image recordings (≥10 wingbeats for each trial) were selected to be analysed.

Treating the DLM, which activates just before the dorsal stroke reversal (Ando and Kanzaki, 2004), as the reference (Kammer, 1971), the cycle length ($\eta$) was defined as the interval between two

adjacent onset DLM spikes corresponding to two adjacent wingbeat cycles (Fig. 3B). The cycle length could be understood as a half-closed–half-open interval, in which the anterior DLM reference spike was included while the posterior one was excluded. The activities of the DVM and 3AXM were expressed by the firing timing relative to the anterior DLM reference spike. The firing timing could be illustrated by the absolute value (named latency, $\tau_{DV}$ and $\tau_{3AX}$, for DVM and 3AXM, respectively) or the relative value (named phase, $\theta_{DV}$ and $\theta_{3AX}$, for DVM and 3AXM, respectively; see Fig. 3B). Phase was calculated as follows: $\theta=360°\times\tau/\eta$. The corresponding bilateral differences in latency and phase, treating the left side as the reference, were exhibited by $\Delta\tau$ and $\Delta\theta$, respectively.

### Statistics

Statistics were approached by individual regressions as well as general linear models (GLMs). In the individual regressions, the least-squares linear regressions were fitted to the data for each individual. The *P*-value (significance level $P<0.05$), the square of the correlation coefficient ($r^2$) and the equation of the correlation line are given. Various GLMs were modelled to test the overall significance of the results for each of the response variables corresponding to the individual regressions, including 'individual' in the model as a random effect. The type III sums of squares were used to evaluate the *P*-values for the effects considering the unbalanced models.

## RESULTS

A total of six male hawkmoths were recorded in this study: two for bilateral DLM–DVM recordings, two for left-side DLM–DVM–3AXM recordings, and two for bilateral 3AXM recordings. They performed free flight manoeuvres for a total 17 trials, exhibiting diverse manoeuvre behaviours. Table 1 lists the groups into which the six individuals were divided for the 17 trials.

### Overview of the time courses of recordings

Within an electromagnetically shielded arena, the male hawkmoths with a ventrally attached telemeter were enticed towards a horizontal cartridge releasing a pheromone plume (Fig. 1). Fig. 2A illustrates one example of a frame from a recording sequence during which the animal was flying in the effective sampling area of the optical system, which had been calibrated by a precision stage. The corresponding process of 3-dimensional reconstruction is shown in Fig. 2B. The quantified wing position showed that at the dorsal side: $\Phi=-63.19\pm1.98°$, $\Psi=-16.14\pm1.45°$, while at the ventral side: $\Phi=15.03\pm6.10°$, $\Psi=31.54\pm4.16°$ (mean ± s.d., $N=20$; wing position data in Fig. 5A were used). The greater variability of the wing position at the ventral stroke reversal indicates that variations in ventral stroke reversal are more likely to be used for flight control than variations in dorsal stroke reversal. After all the key frames of one recording sequence were digitized and reconstructed, the detailed behaviour during free flight manoeuvres was revealed. In the example shown in Fig. 4, the hawkmoth starts steering with a path velocity of 0.29 m s$^{-1}$ horizontally, slows down to 0 m s$^{-1}$ in front of the cartridge, and then accelerates backwards at the end of a collision avoidance behaviour. Comparatively, the path velocity in the vertical plane varies slightly from 0.20 m s$^{-1}$ to 0.09 m s$^{-1}$, as indicated by the time course (Fig. 5A).

Table 1. Division of individuals into groups for trials

| Individual | Number of trials | EMG recordings |
|---|---|---|
| 1 | 5 | Left-side DLM–DVM–3AXM recordings |
| 2 | 3 | |
| 3 | 2 | Bilateral DLM–DVM recordings |
| 4 | 2 | |
| 5 | 2 | Bilateral 3AXM recordings |
| 6 | 3 | |

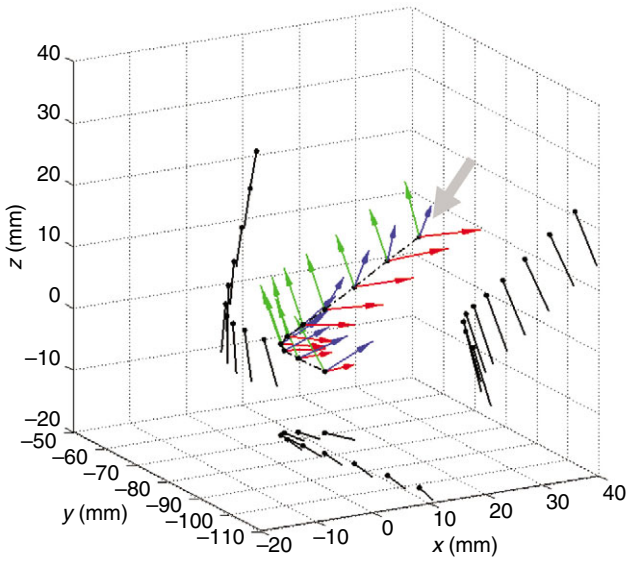


Fig. 4. Flight trajectory and body attitudes during obstacle avoidance manoeuvres (corresponding to the time course in Fig. 5A). Body attitude for every wingbeat of the captured sequence is indicated by the body-fixed frame, of which red, green and blue vectors represent the *x*-, *y*- and *z*-axis in Fig. 2B, respectively. The corresponding orthogonal projections are shown in black, with dots indicating the origins of local frames and lines the body axes (collinear with *y*-axis). The hawkmoth approached the target, performed an avoidance manoeuvre, and then accelerated away by backward flight. The grey arrow indicates the start of this recording.

Fig. 5 plots the three different synchronous recordings, bilateral DLM–DVM, left-side DLM–DVM–3AXM and bilateral 3AXM recordings, by their time courses to interpret illustratively the sequential relationships between wing kinematics and muscle activities. During free flight, the cycle lengths (solid lines with data points marked by open squares), the firing latencies for DVM and 3AXM (broken lines with data points marked by open circles), and the firing phases for DVM and 3AXM (solid lines with data points marked by open circles) are all variable, and all DVM and 3AXM (data points marked by open circles) activate just before the timing of the ventral stroke reversals (data points marked by solid circles). This might suggest certain potential relationships between the mutable wing leading edge angular positions and the mutable timings of DVM and 3AXM onsets, around the timing of the ventral stroke reversals (see statistical analyses below). Considering the alterability of the cycle length (from about 22 ms to 30 ms), the firing timing of latency and phase are not equivalent for DVM and 3AXM (see definitions in Fig. 3B), so that each parameter should be evaluated separately.

When focusing on the bilateral characteristics of free flight, the cycle lengths exhibit reasonable symmetry in the bilateral sides regardless of turning manoeuvres (Fig. 5A). At the same time, the firing timings of latency and phase for DVM (Fig. 5A) and 3AXM

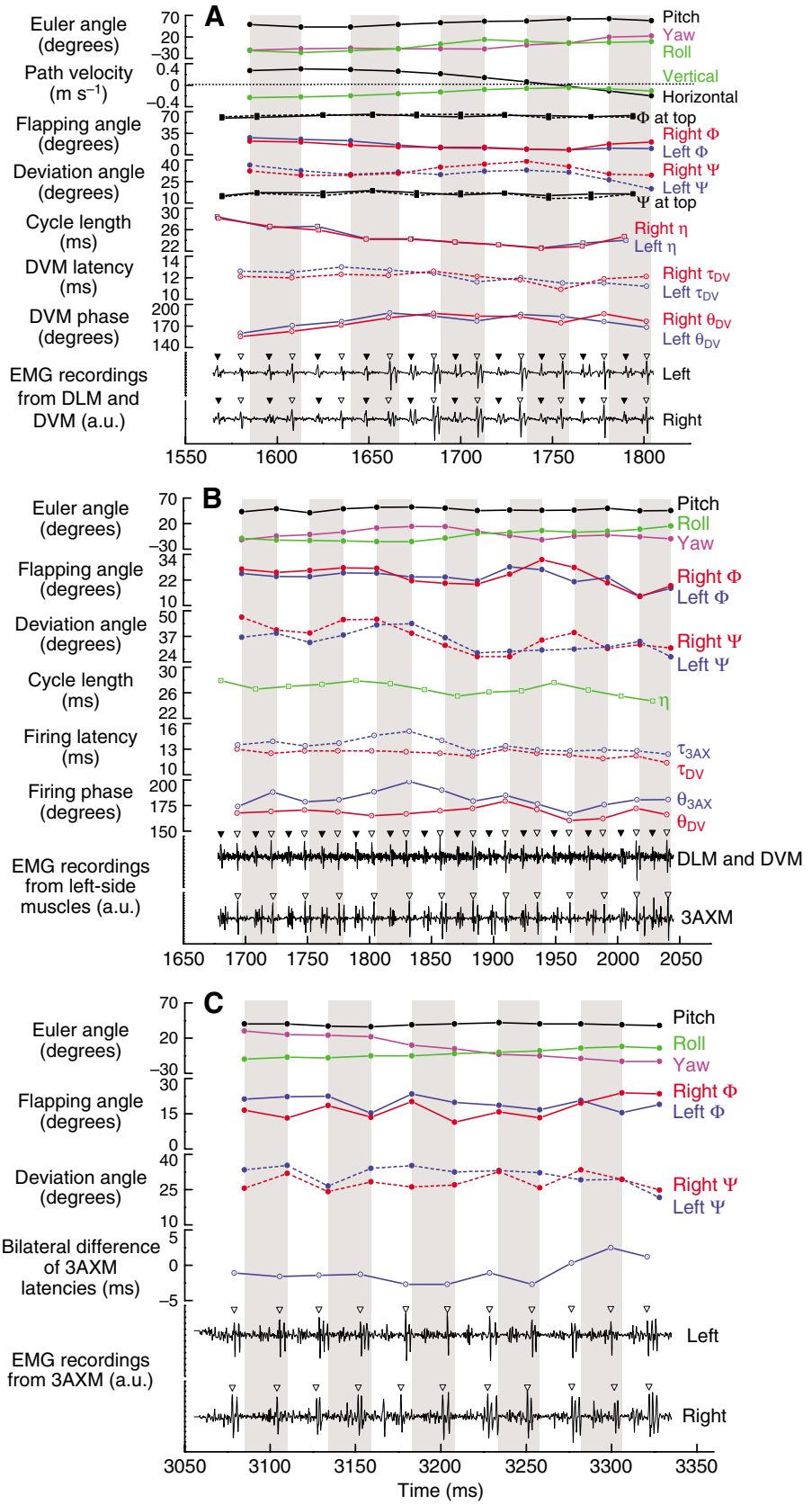


Fig. 5. Time courses for synchronizing analyses on EMG and kinematics. The EMG firing spikes are indicated by the solid arrowheads (for DLM) and open arrowheads (for DVM or 3AXM). Data markers denote different timings by different shapes: open squares for DLM firing timing, open circles for DVM and 3AXM firing timing, solid circles for ventral stroke reversal timing, solid squares for dorsal stroke reversal timing. The alternating white–grey strips are employed to discriminate the time of ventral stroke reversal. The span of the strips does not represent the wingstroke cycle defined by the DLM intervals in Fig. 3B. (A) One case of bilateral DLM–DVM recordings and analysis. The black curves in wing position, as a comparison, denote the flapping and deviation angles (both in inverse values) at the dorsal stroke reversals; solid and dashed lines for right and left side, respectively. (B) One case of left-side DLM–DVM–3AXM recordings and analysis. (C) One case of bilateral 3AXM recordings and analysis. Because of the absence of the DLM reference, only the bilateral latency difference is shown. a.u., arbitrary units.

(Fig. 5C) show relative bilateral asymmetries of DLM. Comparison of the left–right asymmetries of the flapping angle (Φ, solid lines with data points marked by solid circles) and of the deviation angle (Ψ, broken lines with data points marked by solid circles) suggests that the DVM and the 3AXM contribute to steering manoeuvres. The bilateral symmetry of the DLM also indicates its role as a

power muscle to maintain the basic periodic flapping motion (Snodgrass, 1935; Chapman, 1998).

### Analysis of variance for the recordings of wing kinematics and muscle activities

Fig. 6 plots all the data of the left-side DLM–DVM–3AXM recordings, bilateral DLM–DVM recordings and bilateral 3AXM recordings, and the results of the individual regressions. We also combined the data for the six individuals in various GLMs to test the overall significance of the results for each of the response variables ($\Phi$, $\Delta\Phi$, $\Psi$, $\Delta\Psi$ and $\beta$; see Fig. 2B and Fig. 3 for definitions) corresponding to the individual regressions (see Table 2 for models used). All relationships that were significant in the individual regressions also attained overall significance in the GLMs, affirming that the individual regressions did not lead us to overestimate the significance of the results. Levene's test for equality of error variances suggested that the equal variances assumption was fulfilled.

In the GLMs with one covariate, treating wing position ($\Phi$ or $\Psi$) as the response variant (Table 2), the interaction term was not significant in all GLM analyses for wing position, which suggested homogeneity of the relationship between wing position and muscle activity across the level of 'individual'. Correspondingly, the term 'individual' was significant for $\Phi$ (maximum $P$=0.007) and $\Psi$ (maximum $P$=0.039), indicating that the mean values of the wing positions do differ significantly between individuals. For the most significant case of $\Phi$ ($P$<0.001), we can expect the mean flapping angle of the moth indicated by red in Fig. 6A to be 3.215° (95%

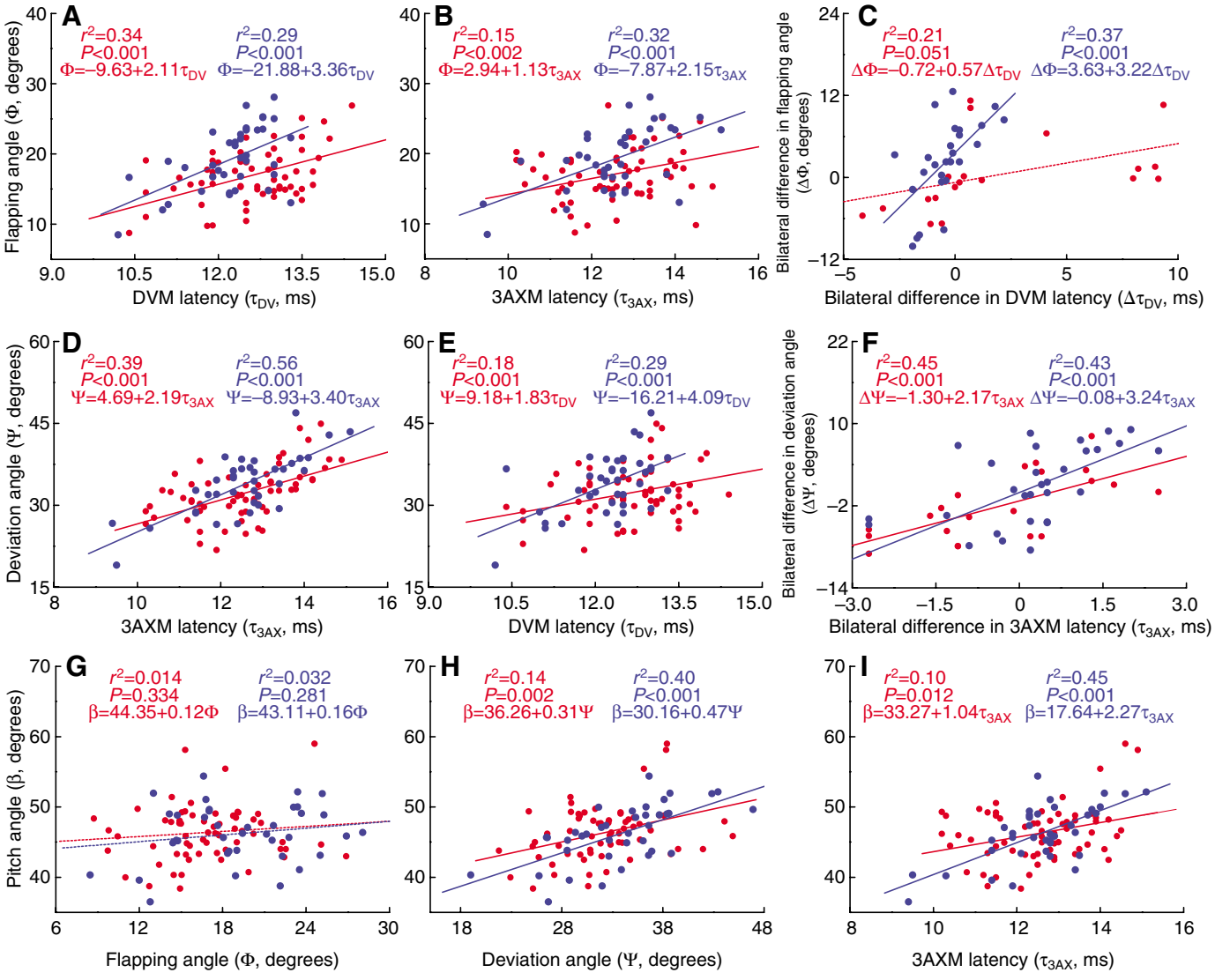


Fig. 6. Individual regressions for the left-side DLM–DVM–3AXM recordings (A,B,D,E,G–I), the bilateral DLM–DVM recordings (C) and the bilateral 3AXM recordings (F). Regression lines are shown by solid lines if the slope of the individual regression was significant and if the covariates ($\tau_{DV}$, $\Delta\tau_{DV}$, $\tau_{3AX}$, $\Delta\tau_{3AX}$, $\Phi$ or $\Psi$) attained overall significance in the corresponding pooled general linear model; otherwise, they are shown by dashed lines. The different colours distinguish data from the different individuals. For each individual, data from several flight sequences were pooled. See Figs 2 and 3 for definitions. (A,B) Graphs of flapping angle $\Phi$ against DVM latency $\tau_{DV}$ (A) and 3AXM latency $\tau_{3AX}$ (B); and (C) graph of bilateral difference in flapping angle $\Delta\Phi$ against bilateral difference in DVM latency $\Delta\tau_{DV}$. (D,E) Graphs of deviation angle $\Psi$ against 3AXM latency $\tau_{3AX}$ (D) and DVM latency $\tau_{DV}$ (E); and (F) graph of bilateral difference in deviation angle $\Delta\Psi$ against bilateral difference in 3AXM latency $\Delta\tau_{3AX}$. (G–I) Graphs of pitch angle $\beta$ against flapping angle $\Phi$ (G), deviation angle $\Psi$ (H) and 3AXM latency $\tau_{3AX}$ (I).

confidence interval: –4.725, –1.705) less than that of the moth indicated by blue. In GLMs treating pitch angle β as the response variant, the term individual was not significant for all models, indicating that the mean values of the pitch angles may be analogous between individuals. The interaction term was not significant in all but one of the GLM analyses for pitch angle ($P$=0.039), with a maximum 4.2% contribution to the total variation, which might not affect the homogeneity of the coefficient for the covariate across the level of 'individual' too much. But in GLM, treating bilateral differences in flapping angle ΔΦ as the response variant, the term 'individual' and interaction were both significant, which was due to the apparent flying behaviour difference in the moth indicated by red in Fig. 6C.

Table 2. Table of $P$-values from the general linear model analyses

| General linear model | Covariate | individual | Interaction | |
|---|---|---|---|---|
| Left-side DLM–DVM–3AXM recordings | | | | |
| $\Phi$= individual+$\tau_{DV}$+$\tau_{DV}$*individual | **<0.001** | **<0.001** | 0.166 | |
| $\Phi$= individual+$\tau_{3AX}$+$\tau_{3AX}$*individual | **<0.001** | **0.007** | 0.101 | |
| $\Psi$= individual+$\tau_{3AX}$+$\tau_{3AX}$*individual | **<0.001** | **0.039** | 0.053 | |
| $\Psi$= individual+$\tau_{DV}$+$\tau_{DV}$*individual | **<0.001** | **0.013** | 0.052 | |
| β= individual+Φ+Φ*individual | 0.150 | 0.586 | 0.834 | |
| β= individual+Ψ+Ψ*individual | **<0.001** | 0.337 | 0.259 | |
| β= individual+$\tau_{3AX}$+$\tau_{3AX}$*individual | **<0.001** | 0.963 | **0.039** | |
| Bilateral DLM–DVM recordings | | | | |
| ΔΦ= individual+Δ$\tau_{DV}$+Δ$\tau_{DV}$*individual | **0.006** | **0.035** | **0.006** | |
| Bilateral 3AXM recordings | | | | |
| ΔΨ=individual+Δ$\tau_{3AX}$+Δ$\tau_{3AX}$*individual | **<0.001** | 0.394 | 0.249 | |
| Left-side DLM–DVM–3AXM recordings | $\tau_{DV}$ | $\tau_{3AX}$ | individual | $\tau_{DV}$*$\tau_{3AX}$ |
| $\Phi$= individual+$\tau_{DV}$+$\tau_{3AX}$+$\tau_{DV}$*$\tau_{3AX}$ | **<0.001** | 0.406 | **<0.001** | 0.784 |
| $\Psi$= individual+$\tau_{DV}$+$\tau_{3AX}$+$\tau_{DV}$*$\tau_{3AX}$ | 0.594 | **<0.001** | 0.070 | 0.754 |

Significant terms ($P$<0.05) in the models are highlighted in bold. The $P$-values for the main effects are calculated using adjusted sums of squares, with only the main effects included in the model. See Figs 2 and 3 for definitions.

### Flapping angle and DVM activity

The flapping angle Φ was positively correlated with the DVM latency $\tau_{DV}$ during free flight (Fig. 6A). This increase was highly significant ($P$<0.001) in the GLM analysis (Table 2), and was just as highly significant in the individual regressions (Fig. 6A). The $r^2$ values of the individual regressions were moderate, with $\tau_{DV}$ explaining 34% and 29% of the within-individual variation in Φ for the two moths (Fig. 6A). The GLM Φ=individual+$\tau_{DV}$ explained a similar proportion of the total variation ($R^2$=0.31). Flapping angle also increased significantly ($P$<0.001) with 3AXM latency $\tau_{3AX}$ in the GLM Φ=individual+$\tau_{3AX}$ (Table 2), and in the individual regressions (Fig. 6B). This is not surprising in the light of the fact that the wingstroke plane generally intersects the local coordinate axes (Fig. 7) that are nearly parallel to the contracting directions of the DVM and the 3AXM, which means that the wing position at the ventral stroke reversal is affected by the two muscles at the same time. But the GLM Φ=individual+$\tau_{DV}$+$\tau_{3AX}$ (Table 2), including both $\tau_{DV}$ and $\tau_{3AX}$ in the model as two covariates, shows a highly significant effect of $\tau_{DV}$ ($P$<0.001) rather than $\tau_{3AX}$ ($P$=0.406). In addition, the term $\tau_{DV}$ explains 15% of the total variation in the GLM, whereas the term $\tau_{3AX}$ explains only 0.7%. These results suggest that the DVM latency $\tau_{DV}$ is one reasonable predictor for the flapping angle Φ of wing position.

Accompanying the positive relationship between the DVM latency and the flapping angle, the bilateral difference in flapping angles ΔΦ was positively correlated with the bilateral difference in DVM latency Δ$\tau_{DV}$ during steering control in free flight. ΔΦ increased significantly ($P$=0.006) with Δ$\tau_{DV}$ in the GLM ΔΦ=individual+Δ$\tau_{DV}$ (see Table 2), but inspection of the individual regressions (Fig. 6C) shows that only the moth indicated by blue expressed a significant effect. The moth indicated by red did not offer clear evidence ($P$=0.051) of a variation in ΔΦ correlated with Δ$\tau_{DV}$, but the data are too widely scattered to discount the possibility that some form of relationship exists. The GLM ΔΦ=individual+Δ$\tau_{DV}$ explained a moderate proportion of the total variation ($R^2$=0.17), which was 13% less than the proportion explained by the corresponding GLM including the significant ($P$=0.006; Table 2) interaction term Δ$\tau_{DV}$*individual ($R^2$=0.30, $P$<0.001). Such individual differences in the underlying slopes are therefore likely to be not negligible in the context of the overall variation in ΔΦ, corresponding to the apparently different flight behaviour in the moth indicated by red (Fig. 6C).

As a result, the linear components of the relationships between Φ and $\tau_{DV}$ and between ΔΦ and Δ$\tau_{DV}$ have been proven statistically.

### Deviation angle and 3AXM activity

Similarly, Fig. 6D,E illustrates the individual regressions of Ψ against 3AXM latency $\tau_{3AX}$ and DVM latency $\tau_{DV}$, and Fig. 6F illustrates the individual regressions of ΔΨ against Δ$\tau_{3AX}$. Deviation angle Ψ was positively correlated with 3AXM latency $\tau_{3AX}$ with high significance ($P$<0.001) in the GLM analysis

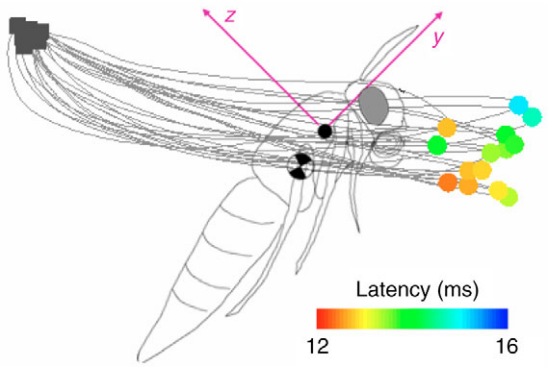


Fig. 7. The left wing tip trajectories projected on the $yoz$ plane in the body-fixed coordinate frame. The data correspond to the time course in Fig. 5B. Assuming that the aerodynamic centre was located at a point 0.25 chord lengths behind the leading edge (Milne-Thomson, 1973; Usherwood and Ellington, 2002), the deviation angles are shifted about 18° along the local $y$-axis backwards to approximate the trajectories of force application point. The wing tips at the ventral stroke reversals are indicated by the colour-mapped circles to denote the 3AXM latency. The wing tips at the dorsal side are marked by the dark grey squares, and the wing base is marked by the black circle. The centre of gravity was estimated by the plumb bob method for body (telemeter attached ventrally) only, neglecting the influence of the relatively light wings.

Table 3. Comparison of the square of the correlation coefficient in the three sequential wingbeat cycles

| $\Delta T$ | $N$ | Trial 1 | | Trial 2 | | Trial 3 | | Trial 4 | | Trial 5 | | Trial 6 | | Trial 7 | | Trial 8 | |
|---|---|---|---|---|---|---|---|---|---|---|---|---|---|---|---|---|---|
| 0 | >12 | 49 | 83 | 46 | 84 | 15 | 65 | 64 | 84 | 72 | 59 | 43 | 78 | 73 | 85 | 30 | 66 |
| 1 | >11 | <1 | 10 | 38 | 28 | <1 | 5 | <1 | 9 | 12 | 20 | 10 | 9 | <1 | 7 | <1 | 4 |
| 2 | >10 | 33 | 14 | 7 | <1 | 3 | 3 | <1 | 15 | <1 | 5 | <1 | 2 | 9 | 15 | <1 | <1 |

Note: $\Delta T$ indicates the cycle delay of the wing kinematics relative to the muscle activities: 0, in phase; 1, the first wingbeat cycle after the current muscle activity; 2, the second wingbeat cycle after the current muscle activity. $N$ indicates the number of data points in each regression. The left column for each trial represents the regression between the flapping angles and the DVM latencies, by means of the square of the correlation coefficient (as a percentage); the right column represents the regression between the deviation angles and the 3AXM latencies. The eight trials here correspond to the left-side DLM–DVM–3AXM recordings.

(Table 2) and in the individual regressions (Fig. 6D). The $r^2$ values of the individual regressions were also moderate, with $\tau_{3AX}$ explaining 39% and 56% of the within-individual variation in $\Psi$ for the two moths (Fig. 6D). The GLM $\Psi$=individual+$\tau_{3AX}$ explained a similar proportion of the total variation ($R^2$=0.44). Also, deviation angle increased significantly ($P$<0.001) with DVM latency $\tau_{DV}$ in the GLM $\Psi$=individual+$\tau_{DV}$ (Table 2), which explained 20% of the total variation, and in the individual regressions (Fig. 6E) with $r^2$ values of 0.18 and 0.29 for the two moths, respectively. However, the GLM with two covariates $\Psi$=individual+$\tau_{DV}$+$\tau_{3AX}$ (Table 2) showed a highly significant effect of $\tau_{3AX}$ ($P$<0.001) rather than $\tau_{DV}$ ($P$=0.594), contrary to the GLM $\Phi$=individual+$\tau_{DV}$+$\tau_{3AX}$. On the other hand, the term $\tau_{3AX}$ explained 31% of the total variation in the GLM, whereas the term $\tau_{DV}$ explained only 0.4%.

As for asymmetrical wing movements in active steering control, a highly significant positive relationship was also found between the bilateral difference in the deviation angles $\Delta\Psi$ and the bilateral difference in 3AXM latency $\Delta\tau_{3AX}$ ($P$<0.001) in the GLM $\Delta\Psi$=individual+$\Delta\tau_{3AX}$ (see the Bilateral 3AXM recordings in Table 2 for models used). The individual regressions (Fig. 6F) were also significant ($P$<0.001), and both showed a positive relationship between $\Delta\Psi$ and $\Delta\tau_{3AX}$. The GLM $\Delta\Psi$=individual+$\Delta\tau_{3AX}$ explained 42% of the total variation in the model.

As a result, the linear components of the relationships between $\Psi$ and $\tau_{3AX}$ and between $\Delta\Psi$ and $\Delta\tau_{3AX}$ have been proven statistically.

### Pitch angle, wing position and muscle activity

The pitch angle was calculated from the key frame of each wingbeat cycle. Fig. 6G,H illustrates the individual regressions of pitch angle $\beta$ against flapping angle $\Phi$ and deviation angle $\Psi$. The slope for both moths indicated by red and blue failed to attain significance ($P$=0.334, $P$=0.281, respectively) for the relationship between $\beta$ and $\Phi$ in the individual regressions (Fig. 6G). Correspondingly, the slope in the GLM $\beta$=individual+$\Phi$ (Table 2) was not significant ($P$=0.150) either. Comparatively, pitch angle $\beta$ was positively correlated with deviation angle $\Psi$ with high significance in the GLM analysis ($P$<0.001; see Table 2) and in the individual regressions ($P$=0.002, $P$<0.001, respectively; see Fig. 6H). The $r^2$ values of the individual regressions were moderate, with $\Psi$ explaining 14% and 40% of the within-individual variation in $\beta$ for the moths indicated by red and blue, respectively (Fig. 6H). The GLM $\beta$=individual+$\Psi$ explained a similar proportion of the total variation ($R^2$=0.23). These results suggest that deviation angle $\Psi$ might be a reasonable predictor of pitch angle $\beta$ during free flight manoeuvres.

Considering the positive linear regression of deviation angle $\Psi$ against 3AXM latency $\tau_{3AX}$, an underlying relationship may exist between pitch angle and 3AXM activities. Highly significant relationships were found between $\beta$ and $\tau_{3AX}$ ($P$<0.001) in the GLM $\beta$=individual+$\tau_{3AX}$ (see Table 2). The individual regressions were also significant ($P$<0.001) for the moth indicated by blue, and showed a positive relationship between $\beta$ and $\tau_{3AX}$ (Fig. 6I). As for the moth indicated by red, the individual regressions were still significant as $P$=0.012 for $\tau_{3AX}$. The GLM $\beta$=individual+$\tau_{3AX}$ explained a moderate proportion of the total variation ($R^2$=0.21), and explained only slightly less of the total variation than the equivalent GLM including the significant ($P$=0.039; Table 2) interaction term $\tau_{3AX}$*individual ($R^2$=0.24), which suggests the individual differences in the underlying slopes that may exist are therefore likely to be small in the context of the overall variation in pitch angle.

As a result, the inter-periodic variation of the pitch angle at the ventral stroke reversal with respect to the firing latency of the 3AXM has been traced through the deviation angle, and the linear component of their relationship has been proven statistically.

### Verification of independence over time series

The two specific flight muscles investigated in the present study, the DVM and the 3AXM, are both synchronous (neurogenic) muscles (Kammer, 1971). Though the power output of these synchronous flight muscles contributes to the current wingbeat (Tu and Daniel, 2004), it is also possible that the current muscle activities can affect the subsequent wingbeats. This increases the difficulty in the statistical analysis of the EMG recordings, which are the non-independent time series. Here we simply compared the contributions of the current DVM and 3AXM activities with the current and the subsequent two wingbeats (Table 3) by means of the square of the correlation coefficient ($r^2$), which represent the contributions of predictors to the response. The results confirm that the current muscle activities mainly contribute to the current wingbeat cycle, and suggest that the least-squares linear regressions and GLM analyses, treating the simultaneous recordings of wing kinematics and muscle activity as the independent time series, were reasonable.

## DISCUSSION

In the present study, six male hawkmoths were investigated telemetrically. The linear component of the relationship between wing kinematics (wing position described by the flapping angle and the deviation angle in a body-fixed coordinate frame) and muscle activity (firing latency of the DVM and the 3AXM) were proven statistically. The inter-periodic variation of the pitch angle at the ventral stroke reversal with respect to the firing latency of the 3AXM was traced through the deviation angle, and the linear component of their relationship was proven statistically. At the same time, the linear component of the relationship between the bilateral differences in wing kinematics and in muscle activity were additionally investigated and also proven statistically.

In this discussion, we hypothesize about the functions of the two investigated muscles in active flight control based on the statistical results, then discuss the common issue of behaviour in free flight and the possible effects due to the employed telemeter. We also discuss prospects for future research in freely flying insects.

### Functions of the DVM and the 3AXM in active flight control

It is widely thought that the direct muscles are steering muscles that affect the kinematics of the wingstroke, while the indirect muscles are power muscles that maintain the periodic flapping motion to supply the propulsive effort (Snodgrass, 1935; Chapman, 1998). In the present study, both the DVM (an indirect muscle) and the 3AXM (a direct muscle) exhibited a significant linear relationship with the wing kinematics (Fig. 6A–F, Table 2). The closer relationship of the 3AXM than of the DVM may stem from the different muscle types. A direct muscle can actuate the appendage of a wing directly, while the wing movement due to an indirect muscle may also be affected by other factors such as the elastic properties of muscles and of the exoskeleton. According to the linear relationships expressed in the statistical results, the stroke depth along the direction of the flapping angle is modulated by the firing latency of the DVM, while that along the direction of the deviation angle is modulated by the firing latency of the 3AXM. They both perform as a brake to constrain the wing downstroke initiated by the DLM along the two directions. Modulating the firing latencies will affect the downstroke depth accompanying potential variations in stroke amplitude and stroke plane.

Representing the wing leading edge position at the ventral stroke reversal, the flapping angle and the deviation angle investigated in this study are two important factors in determining the mean stroke plane. At the same time, the pitch angle varies in association with the normal stroke plane during acceleration or deceleration. The GLMs (Table 2) and individual regressions (Fig. 6G,H) confirm that a potential relationship exists between the pitch angle and the deviation angle rather than the flapping angle. Further analyses (Fig. 6I, Table 2) show that the pitch angle varies with the firing latency, which is derived from the relationship between the deviation angle and the firing latency. Fig. 7 shows the projection of the wing trajectory on the *yoz* plane in the body-fixed coordinate system, and the corresponding deviation angle as well as the 3AXM latency (shown in colour-coded circles). Presumably, the pitch angle in the key frame may be affected by the integral of the pitch moment during downstroke. The downstroke generated nose-up torque while the upstroke generated nose-down torque, but the latter value is less than the former because the downstroke trajectory is far away from the centre of gravity, which led to a greater lever of force. This indicates that the pitch angle at the ventral reversal is mainly determined by the downstroke. Increasing the 3AXM latency would move the wing leading edge more ahead, which increases the possibility of enhancing the nose-up torque.

The functions of the DVM and the 3AXM in active flight control are also expressed in bilateral steering. Bilateral differences in wing kinematics will lead to bilateral steering or compensate for the bilateral disturbance in longitudinal flights. Though there is no clear evidence that an insect can modulate roll and yaw separately and the most common mode of turning is the banked turn, in which roll and yaw are advantageously coupled to reduce the turning circle (Taylor, 2001), a hawkmoth might roll or yaw mutually independently (see Fig. 5A), which indicates different muscles may contribute differently to roll and yaw control. The linear relationships between the bilateral difference in flapping angle $\Delta\Phi$ and the bilateral difference in DVM latency $\Delta\tau_{DV}$, and between the bilateral difference in deviation angle $\Delta\Psi$ and the bilateral difference in 3AXM latency $\Delta\tau_{3AX}$ are both significant (see Table 2). In the recording time courses (Fig. 5), though we could not find the quantitative relationship between the change rate of roll and yaw and the bilateral difference in wing position, the cross-correlation analysis (Table 4) may give some qualitative results. It is difficult to determine whether the roll and yaw angles are separately related to the bilateral difference in the flapping and deviation angles, but the relationship between $S_{\Delta\Phi}$ and $S_{dRoll}$ and between $S_{\Delta\Psi}$ and $S_{dYaw}$ are relatively stable. Here dRoll and dYaw are the variation of Roll and Yaw, respectively, from the previous sampling to the current; $S_{dRoll}$ and $S_{dYaw}$ are the signs of dRoll and dYaw, respectively, which represent qualitatively the changing tendency of the corresponding Euler angles; $S_{\Delta\Phi}$ and $S_{\Delta\Psi}$ are the signs of $\Delta\Phi$ and $\Delta\Psi$ (see Fig. 3 for definitions), respectively, which represent the bilateral difference in wing position qualitatively. The negative coefficients of $S_{\Delta\Phi}$ relative to $S_{dRoll}$ indicate that the rotation around the roll axis tends to the side with smaller flapping angle, while the positive coefficients of $S_{\Delta\Psi}$ relative to $S_{dYaw}$ indicate the rotation around the yaw axis tends to the side with the smaller deviation angle (see also the definitions in Fig. 2B). At the same time, the response lag from one to two cycles might be due to the inertia forces during free flight (Fry et al., 2003). Considering the relationships between yaw and $\Delta\Psi$ and between roll and $\Delta\Phi$, respectively, and the relationships between $\Delta\Psi$ and $\Delta\tau_{3AX}$ and between $\Delta\Phi$ and $\Delta\tau_{DV}$, respectively, this suggests that the 3AXM might mainly contribute to yaw control while the DVM mainly contributes to roll control in the local body-fixed frame.

### Behavioural difference in the free flying hawkmoths

Hawkmoths can express all kinds of flight behaviours (Stevenson et al., 1995; Willis and Arbas, 1991). In free flight experiments, it is impossible to observe two identical flight behaviours even for the same animal, let alone for different individuals. Individual differences may be the main reason for behavioural differences. In this study, six hawkmoths from 2 to 4 days old were investigated.

Table 4. Qualitative analysis of the bilateral difference in wing position and the change in Euler angle by cross-correlation

| | $S_{\Delta\Phi}$–$S_{dRoll}$ | | $S_{\Delta\Phi}$–$S_{dYaw}$ | | $S_{\Delta\Psi}$–$S_{dRoll}$ | | $S_{\Delta\Psi}$–$S_{dYaw}$ | |
|---|---|---|---|---|---|---|---|---|
| Case | Lag | Coeff. | Lag | Coeff. | Lag | Coeff. | Lag | Coeff. |
| 1 | 2 | –0.735 | –5 | –0.522 | 2 | –0.490 | 2 | 0.689 |
| 2 | 1 | –0.724 | 1 | 0.970 | 1 | –0.724 | 1 | 0.970 |
| 3 | 1 | –0.463 | 1 | 0.591 | –3 | 0.401 | 2 | 0.525 |

Note: the data in Fig. 5A, B and C were used for case 1, 2 and 3, respectively. $S_{\Delta\Phi}$ and $S_{\Delta\Psi}$ are the signs of $\Delta\Phi$ and $\Delta\Psi$ (see Fig. 3 for definitions), respectively, which represent the bilateral difference in wing position qualitatively. dRoll and dYaw are the variation of roll and yaw, respectively, from the previous sampling to the current. $S_{dRoll}$ and $S_{dYaw}$ are the signs of dRoll and dYaw, respectively, which represent qualitatively the changing tendency of the corresponding Euler angles. In the cross-correlation analysis, Lag indicates the lag of the changing tendency of the Euler angle response to the bilateral difference in wing position; Coeff., the corresponding correlation coefficient. The maximum range of positive and negative lags for a series was set as 5, and only the maximum coefficient (absolute value) and the corresponding lag are listed here. The negative value of lag indicates advance and the negative value of coefficient indicates decreasing Euler angle accompanying the positive bilateral difference in wing position, and *vice versa*.

The largest one weighed 1.22 g (including a telemeter) with a wingspan of 41 mm, while the smallest one weighed 1.10 g with a wingspan of 35 mm. The attachment of a 0.23 g transmitter is another reason for behavioural differences, and whether a transmitter is attached or not should be a fixed factor in the GLM analysis. However, in the present study, we focused on the relationship between wing kinematics and muscle activity. To obtain the EMG signal of muscle activity during free flight, attaching a transmitter was necessary. Insects have a good capability for takeoff (Marden, 1987) and some can even lift up to three times their mass. Based on our observations, the hawkmoth *Agrius convolvuli* could fly with up to 1.4 times the original body weight. The added weight due to the attached telemeter occupied on average 24% of the body weight of the tested animals, which was not far from the changes of body weight of a hawkmoth under natural conditions. Additionally, in the preparation of each animal, the telemeter was attached ventrally, at the same position in each animal (near the centre of gravity of the animal), to make the potential effect of the telemeter equivalent for each individual and to avoid increasing the between-individual variation in GLMs. The slight difference of attachment could be treated as one part of the individual differences. Thus, ignoring the effects of the attachment of a transmitter will not compromise our analyses and results in this free flight study.

The factor of the individual does affect the flight variables significantly, especially for the flapping angle and the deviation angle (maximum $P$=0.007 and 0.039, respectively; see Table 2). The average wing position for each animal is significantly different, which may be attributed to individual differences in the structural constraint of a wing base or to individual differences in the ability to generate aerodynamic forces related to wing size and body weight. For instance, a light moth with large wings may produce enough lift to support weight more easily (with a smaller wingstroke amplitude, for example) than a heavier moth with small wings. Actually, in the left-side DLM–DVM–3AXM recordings we can expect the flapping angle of the moth indicated by red (body weight: 1.19 g, wingspan: 41 mm) to be 3.215° less than that of the moth indicated by blue (body weight: 1.22 g, wingspan: 41 mm) with a high significance ($P$<0.001; see Table 2 and Fig. 6A). Additionally, the factor of the individual may influence the relationships between wing kinematics and muscle activity. Though it shows no significant effect over the linear relationships between the flapping angle and the corresponding covariates and between the deviation angle and the corresponding covariates (see Table 2), the factor of the individual may affect the linear relationship between the pitch angle and the 3AXM latency ($P$=0.039, though such individual differences in the underlying slope are small). In the case of the bilateral DLM–DVM recording, the factor of the individual affects the relationship between $\Delta\Phi$ and $\Delta\tau_{DV}$ deeply. It seems not to be an artifact but a quite different flight behaviour from the same animal in free flight.

There are probably several unknown factors (such as the aerodynamic effects and other muscles) involved in active flight control that were not investigated in this study. The total variation due to omitting the unknown factors or covariates in the models might be so remarkable as to outweigh the between-individual variation due to individual differences. There are more than enough independent kinematic inputs to permit active flight control, although it is equally possible that one or more of these inputs is redundant and is simply used to provide finer control of manoeuvres (Taylor, 2001). Besides the flapping angle and the deviation angle (tested here), other kinematics such as abdominal deflection (Zanker, 1988) may also contribute to pitch angle and free flight manoeuvres. Correspondingly, besides the 3AXM, another muscle related to abdominal deflection may also be found to be valuable for pitch control. Because of its redundant control system, a hawkmoth can utilize an alternative subset of controls to handle the flight mission on hand, which exhibits a multiplicity of active flight controls and behavioural differences.

We gratefully acknowledge Professor Kenji Kiguchi and Dr Koji Shirai for their support and advice in rearing hawkmoths; Dr Stacey Combes for her advice about the free flight behaviours of hawkmoths; Dr Evan S. Hill for improving the readability of the manuscript; and two anonymous reviewers for the constructive comments. This work is supported by the Grant-in-Aid for Scientific Research from Japan Society for the Promotion of Science (H.W.) and the Japan Ministry of Education, Culture, Sports, Science and Technology (R.K.; 18100002), and the Grant- in-Aid for younger researchers from RCAST, the University of Tokyo (N.A.).

## REFERENCES

**Ando, N. and Kanzaki, R.** (2004). Changing motor patterns of the 3rd axillary muscle activities associated with longitudinal control in freely flying hawkmoths. *Zool. Sci.* **21**, 123-130.
**Ando, N., Shimoyama, I. and Kanzaki, R.** (2002). A dual-channel FM transmitter for acquisition of flight muscle activities from the freely flying hawkmoth, *Agrius convolvuli*. *J. Neurosci. Methods* **115**, 181-187.
**Burkhardt, D.** (1977). On the vision of insects. *J. Comp. Physiol.* **120**, 33-50.
**Chapman, R. F.** (1998). Mechanisms of wing movement. In *The Insects: Structure and Function*, pp. 198-201. London: Cambridge University Press.
**Eaton, J. L.** (1971). Morphology of the head and thorax of the adult tobacco hornworm, *Manduca sexta* (Lepidoptera: Sphingidae). 1. Skeleton and muscles. *Ann. Entomol. Soc. Am.* **64**, 437-445.
**Fischer, H. and Kutsch, W.** (1999). Timing of elevator muscle activity during climbing in free locust flight. *J. Exp. Biol.* **202**, 3575-3586.
**Fry, S. N., Sayaman, R. and Dickinson, M. H.** (2003). The aerodynamics of free-flight maneuvers in *Drosophila*. *Science* **300**, 495-498.
**Haslwanter, T.** (1995). Mathematics of three-dimensional eye rotations. *Vision Res.* **35**, 1727-1739.
**Hedwig, H. and Becher, G.** (1998). Forewing movements and intracellular motoneurone stimulation in tethered flying locusts. *J. Exp. Biol.* **201**, 731-744.
**Kammer, A. E.** (1971). The motor output during turning flight in a hawkmoth, *Manduca sexta*. *J. Insect Physiol.* **17**, 1073-1086.
**Kanzaki, R., Arbas, E. A., Strausfeld, N. J. and Hildebrand, J. G.** (1989). Physiology and morphology of projection neurons in the antennal lobe of the male moth *Manduca sexta*. *J. Comp. Physiol. A* **165**, 427-453.
**Kutsch, W.** (2002). Transmission of muscle potentials during free flight of locusts. *Comput. Electron. Agric.* **35**, 181-199.
**Kutsch, W., Berger, S. and Kautz, H.** (2003). Turning manoeuvres in free-flying locusts: two-channel radio-telemetric transmission of muscle activity. *J. Exp. Zool.* **299**, 139-150.
**Marden, J. H.** (1987). Maximum lift production during takeoff in flying animals. *J. Exp. Biol.* **130**, 235-258.
**Milne-Thomson, L. M.** (1973). *Theoretical Aerodynamics*. New York: Dover Publications.
**Rheuben, M. B. and Kammer, A. E.** (1987). Structure and innervation of the third axillary muscle of *Manduca* relative to its role in turning flight. *J. Exp. Biol.* **131**, 373-402.
**Schilstra, C. and Hateren, J. H.** (1998). Stabilizing gaze in flying blowflies. *Nature* **395**, 654.
**Snodgrass, R, E.** (1935). *Principles of Insect Morphology*. New York: McGraw-Hill.
**Stevenson, R. D., Corbo, K., Baca, L. B. and Le, Q. D.** (1995). Cage size and flight speed of the tobacco hawkmoth *Manduca sexta*. *J. Exp. Biol.* **198**, 1665-1672.
**Taylor, G. K.** (2001). Mechanics and aerodynamics of insect fight control. *Biol. Rev.* **76**, 449-471.
**Tu, M. S. and Daniel, T. L.** (2004). Submaximal power output from the dorsolongitudinal flight muscles of the hawkmoth *Manduca sexta*. *J. Exp. Biol.* **207**, 4651-4662.
**Tu, M. S. and Dickinson, M. H.** (1996). The control of wing kinematics by two steering muscles of the blowfly (*Calliphora vicina*). *J. Comp. Physiol. A* **178**, 813-830.
**Usherwood, J. R. and Ellington, C. P.** (2002). The aerodynamics of revolving wings. I. Model hawkmoth wings. *J. Exp. Biol.* **205**, 1547-1564.
**Wang, H., Zeng, L. J., Liu, H. and Yin, C. Y.** (2003). Measuring wing kinematics, flight trajectory, and body attitude during forward flight and turning maneuvers in dragonflies. *J. Exp. Biol.* **206**, 745-757.
**Willis, M. A. and Arbas, E. A.** (1991). Odor-modulated upwind flight of the sphinx moth, *Manduca sexta* L. *J. Comp. Physiol. A* **169**, 427-440.
**Willmott, A. P. and Ellington, C. P.** (1997). The mechanics of flight in the hawkmoth *Manduca sexta*. I. Kinematics of hovering and forward flight. *J. Exp. Biol.* **200**, 2705-2722.
**Wilson, D. N. and Weis-Fogh, T.** (1962). Patterned activity of coordinated motor units, studied in flying locusts. *J. Exp. Biol.* **39**, 643-667.
**Wolf, H.** (1990). On the function of a locust flight steering muscle and its inhibitory innervation. *J. Exp. Biol.* **150**, 55-80.
**Zanker, J. M.** (1988). How does lateral abdomen deflection contribute to flight control of *Drosophila melanogaster*? *J. Comp. Physiol. A* **162**, 581-588.